

Noise Resilience of an RGNG-based Grid Cell Model

Jochen Kerdels and Gabriele Peters

University of Hagen, Universitätsstrasse 1, D-58097 Hagen, Germany

Keywords: Noise Resilience, Grid Cell Model, Input Space Representation, Recursive Growing Neural Gas.

Abstract: Grid cells are neurons in the entorhinal cortex of mammals that are known for their peculiar, grid-like firing patterns. We developed a generic computational model that describes the behavior of neurons with such firing patterns in terms of a competitive, self-organized learning process. Here we investigate how this process can cope with increasing amounts of noise in its input signal. We demonstrate, that the firing patterns of simulated neurons are mostly unaffected with regard to their structure even if high levels of noise are present in the input. In contrast, the maximum activity of the corresponding neurons decreases significantly with increasing levels of noise. Based on these results we predict that real grid cells can retain their triangular firing patterns in the presence of noise, but may exhibit a noticeable decrease in their peak firing rates.

1 INTRODUCTION

Several regions of the mammalian brain contain neurons that exhibit peculiar, grid-like firing patterns (Fyhn et al., 2004; Hafting et al., 2005; Boccara et al., 2010; Killian et al., 2012; Yartsev et al., 2011; Domnisoru et al., 2013; Jacobs et al., 2013). The most common example for such neurons are so-called *grid cells* found in the medial entorhinal cortex (MEC) of rat (Fyhn et al., 2004; Hafting et al., 2005). The activity of these cells correlates with the animal's location in a periodic, triangular pattern that spans across the entire environment of the animal.

We developed a generic computational model that is able to describe the behavior of neurons with such grid-like firing patterns (Kerdels and Peters, 2013; Kerdels and Peters, 2015b; Kerdels, 2016). Here we investigate how this model reacts to random noise in its input signal as it would be expected to occur in natural neurobiological circuits where each neuron receives input from hundreds to thousands of other neurons (Koch, 2004)¹.

The next section summarizes our grid cell model briefly and highlights those mechanisms of the model that are especially relevant to the investigation of input signal noise. Subsequently, section 3 outlines how scalable amounts of noise are added to the input signal of our grid cell model. Section 4 then reports and analyses the results obtained from simulation runs

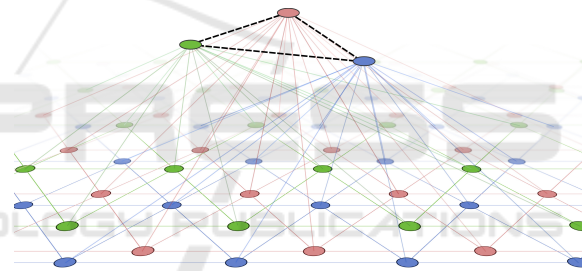


Figure 1: Illustration of the RGNG-based neuron model. The top layer is represented by three units (red, green, blue) connected by dashed edges. The prototypes of the top layer units are themselves RGNGs. The units of these RGNGs are illustrated in the second layer by corresponding colors.

with varying levels of noise. Finally, we discuss our findings in section 5.

2 GRID CELL MODEL

We developed a generic neuron model that is able to describe, among others, the behavior of grid cells (Kerdels, 2016). At its core the model uses the *recursive growing neural gas* (RGNG) algorithm to describe the collective behavior of a group of neurons. The RGNG algorithm extends the regular growing neural gas (GNG) algorithm proposed by Fritzke (Fritzke, 1995) in a recursive fashion². A reg-

²A formal definition of the RGNG algorithm is provided in the appendix.

¹p. 411ff

ular GNG is an unsupervised learning algorithm that approximates the structure of its input space with a network of units where each unit represents a local region of input space while the network itself represents the input space topology. In a *recursive* GNG or RGNG the units can not only represent local input space regions but may also represent entire RGNGs themselves resulting in a layered, hierarchical structure of interleaved input space representations.

In our grid cell model we use a single RGNG with two layers to model a group of neurons (Fig. 1). The units in the top layer (TL) represent the individual cells of the group. Each of these TL units contains an RGNG located in the bottom layer (BL). These BL-RGNGs can be interpreted as the dendritic trees of the neurons, each of which learning a separate representation of the entire input space. The units of the BL-RGNGs correspond to local subsections of the dendritic tree that recognize input patterns from specific, local regions of input space. In the model, these local regions are represented by so-called *reference vectors* or *prototypes*. Thus, each modelled neuron (TL unit) has a set of prototypes (BL units) that are arranged in a network (BL RGNG) that constitutes a piecewise approximation of the neuron’s input space. The neurons (TL units) themselves are organized in a network (TL RGNG) as well resulting in an interleaved arrangement of the individual input space approximations.

Please note that the term “neuron” is used differently here compared to its regular usage in a growing neural gas context. It is used synonymously only with the TL units of the model and not the BL units. Furthermore, the RGNG is inherently different from existing hierarchical versions of the growing neural gas like those proposed by, e.g., Doherty et al. (Doherty et al., 2005) or Podolak and Bartocha (Podolak and Bartocha, 2009). These approaches represent the input space in a hierarchical fashion with every unit of the hierarchical GNG corresponding to a single local region of input space. In our model, this holds true only for the BL units whereas every TL unit represents the *entire* input space.

2.1 Learning

The two-layer RGNG used in the grid cell model has no explicit training phase and updates its input space approximation continuously. In a first step, each input ξ is processed by all neurons. To this end every neuron determines the best and second best matching units (BMUs) termed s_1 and s_2 , respectively. Units s_1 and s_2 are those BL units whose prototypes $s_{1,w}$ and $s_{2,w}$ are closest to the input ξ according to a dis-

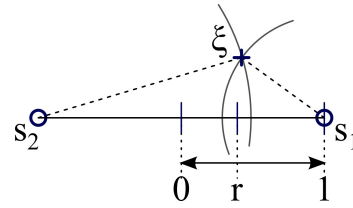


Figure 2: Geometric interpretation of ratio r , which is used as basis for an approximation of the top layer unit’s “activity”.

tance function D . Once determined, the BMUs of every neuron are adapted towards the input ξ and the corresponding BL networks are updated where necessary.

In a second step, the single neuron whose BMU was closest to the input and its direct neighboring neurons in the TL network are allowed to adapt towards the input a second time. This selective adaptation aligns the input space representations of the individual neurons and interleaves them evenly to cover the input space as well as possible (Kerdels, 2016).

2.2 Activity Approximation

The RGNG-based model describes a group of neurons for which we would like to derive their “activity” for any given input as a scalar that represents the momentary firing rate of the particular neuron. Yet, the RGNG algorithm itself does not provide a direct measure that could be used to this end. Therefore, we derive the activity a_u of a modelled neuron u based on the neuron’s best and second best matching BL units s_1 and s_2 with respect to a given input ξ as:

$$a_u := e^{-\frac{(1-r)^2}{2\sigma^2}},$$

with $\sigma = 0.2$ and ratio r :

$$r := \frac{D(s_{2,w}, \xi) - D(s_{1,w}, \xi)}{D(s_{1,w}, s_{2,w})}, \quad s_1, s_2 \in u.w.U,$$

using a distance function D . Figure 2 provides a geometric interpretation of the ratio r . If input ξ is close to BMU s_1 in relation to s_2 , ratio r becomes 1. If on the other hand input ξ has about the same distance to s_1 as it has to s_2 , ratio r becomes 0.

This measure of activity allows to correlate the response of a neuron to a given input with further variables. An example of such a correlation is shown in figure 3b as a *firing rate map*, which correlates the animal’s location (Fig. 3a) with the activity of a simulated grid cell at that location. The firing rate maps resulting from our simulations are constructed

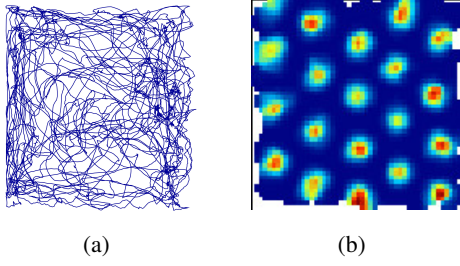


Figure 3: (a) Example trace of rat movement within a rectangular, $1\text{ m} \times 1\text{ m}$ environment recorded for a duration of 10 minutes. Movement data published by Sargolini et al. (Sargolini et al., 2006). (b) Color-coded firing rate map of a simulated grid cell ranging from dark blue (no activity) to red (maximum activity).

according to the procedures described by Sargolini et al. (Sargolini et al., 2006) but using a 5×5 boxcar filter for smoothing instead of a Gaussian kernel as introduced by Stensola et al. (Stensola et al., 2012). This conforms to the de facto standard of rate map construction in the grid cell literature. Each rate map integrates position and activity data over 30000 time steps corresponding to a single experimental trial with a duration of 10 minutes recorded at 50Hz.

3 INPUT SIGNAL

In general, the RGNG-based neuron model is independent of any specific type of input space and can process arbitrary input signals. However, only input spaces with certain characteristics will cause the modelled neurons to exhibit grid-like firing patterns with respect to a given variable, e.g., the animal's location. More precisely, grid-like firing patterns will only emerge if the input signals originate from a uniformly distributed, two-dimensional manifold in the input space that correlates with the respective external variable.

In the case of grid cells there are many conceivable input spaces that meet these requirements (Kerdels, 2016). For our experiments we choose an input space where the position of the animal is encoded by two vectors as shown in figure 4. The two-dimensional position is represented by the activity of two sets of cells that each are connected in a one-dimensional, periodic fashion like, e.g., a one-dimensional ring attractor network. Similar types of input signals for grid cell models were proposed in the literature by, e.g., Mhatre et al. (Mhatre et al., 2010) as well as Pilly and Grossberg (Pilly and Grossberg, 2012).

For the experiments discussed below the input signal $\xi := (v^x, v^y)$ is implemented as two concatenated 50-dimensional vectors v^x and v^y . To generate an in-

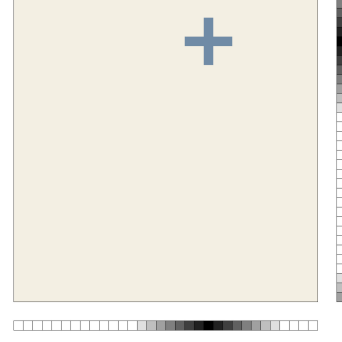


Figure 4: The input signal for our experiments is derived by encoding a position (blue cross) in a periodic, two-dimensional input space (square) as the activity (black = high, white = low) of two sets of cells (vertical and horizontal groups of small boxes) that each are connected in a one-dimensional, periodic fashion, i.e., the activity wraps around at the borders of the resulting vectors.

put signal a position $(x, y) \in [0, 1] \times [0, 1]$ is read from traces (Fig. 3a) of recorded rat movements that were published by (Sargolini et al., 2006) and mapped onto the corresponding elements of v^x and v^y as follows:

$$v_i^x := \max \left(1 - \left| \frac{i - \lfloor dx + 0.5 \rfloor}{s} \right|, 1 - \left| \frac{d + i - \lfloor dx + 0.5 \rfloor}{s} \right|, 0 \right),$$

$$v_i^y := \max \left(1 - \left| \frac{i - \lfloor dy + 0.5 \rfloor}{s} \right|, 1 - \left| \frac{d + i - \lfloor dy + 0.5 \rfloor}{s} \right|, 0 \right),$$

$$\forall i \in \{0 \dots d - 1\},$$

with $d = 50$ and $s = 8$. The parameter s controls the slope of the activity peak with higher values of s resulting in a broader peak.

Each input vector $\xi := (\tilde{v}^x, \tilde{v}^y)$ was then augmented by noise as follows:

$$\tilde{v}_i^x := \max[\min[v_i^x + \xi_n(2U_{\text{rnd}} - 1), 1], 0],$$

$$\tilde{v}_i^y := \max[\min[v_i^y + \xi_n(2U_{\text{rnd}} - 1), 1], 0],$$

$$\forall i \in \{0 \dots d - 1\},$$

with maximum noise level ξ_n and uniform random values $U_{\text{rnd}} \in [0, 1]$. The rationale for this noise model is as follows. Each element of the input vector rep-

represents the normalized firing rate of an input neuron, where typical peak firing rates of neurons in the parahippocampal-hippocampal region range between 1Hz and 50Hz (Hafting et al., 2005; Sargolini et al., 2006; Boccara et al., 2010; Krupic et al., 2012). Some proportion of this firing rate is due to spontaneous activity of the corresponding neuron. According to Koch (Koch, 2004) this random activity can occur about once per second, i.e., at 1Hz. Hence, the proportion of noise in the normalized firing rate resulting from this spontaneous firing can be expected to lie between 1.0 and 0.02 given the peak firing rates stated above. As we have no empirical data on the distribution of peak firing rates in the input signal of grid cells we assume a uniform distribution. The parameter ξ_n allows to control the maximum noise level or the assumed minimal peak firing rate (implicitly). For example, a maximum noise level of $\xi_n = 0.1$ corresponds to a minimal peak firing rate of 10Hz, and a level of $\xi_n = 0.5$ corresponds to a minimal peak firing rate of 2Hz.

4 SIMULATION RESULTS

To investigate how the RGNG-based grid cell model reacts to noise in its input signal we ran a series of simulations with increasing levels ξ_n of noise (or, correspondingly, decreasing minimal peak firing rates). All simulation runs used the fixed set of parameters shown in table 1 (appendix). Both, the number $\theta_1 \cdot M = 100$ of simulated grid cells as well as the number $\theta_2 \cdot M = 20$ of dendritic subsections per cell are chosen to lie within a biologically plausible range. The latter number can be estimated based on the morphological properties of MEC layer II stellate cells, which are presumed to be one type of principal neurons that exhibit grid-like firing patterns (Giocomo et al., 2007; Giocomo and Hasselmo, 2008). The dendritic tree of these neurons has about 7500 to 15000 spines, each hosting one or more synaptic connections (Lingenhl and Finch, 1991). In our experiments we assume that the input space of each grid cell is comprised by the output of 100 input neurons and that each grid cell recognizes $\theta_2 \cdot M = 20$ different input patterns originating from that space. This parametrization results in 3.75 to 7.5 available spines for each input dimension in a prototype pattern. This is a conservative choice that provides some margin for possible variability in input dimension and number of prototypes. Estimating the number $\theta_1 \cdot M$ of grid cells in a grid cell group³ is more difficult. Sten-

³Grid cells are organized in groups that share the same grid spacing and grid orientation (Stensola et al., 2012).

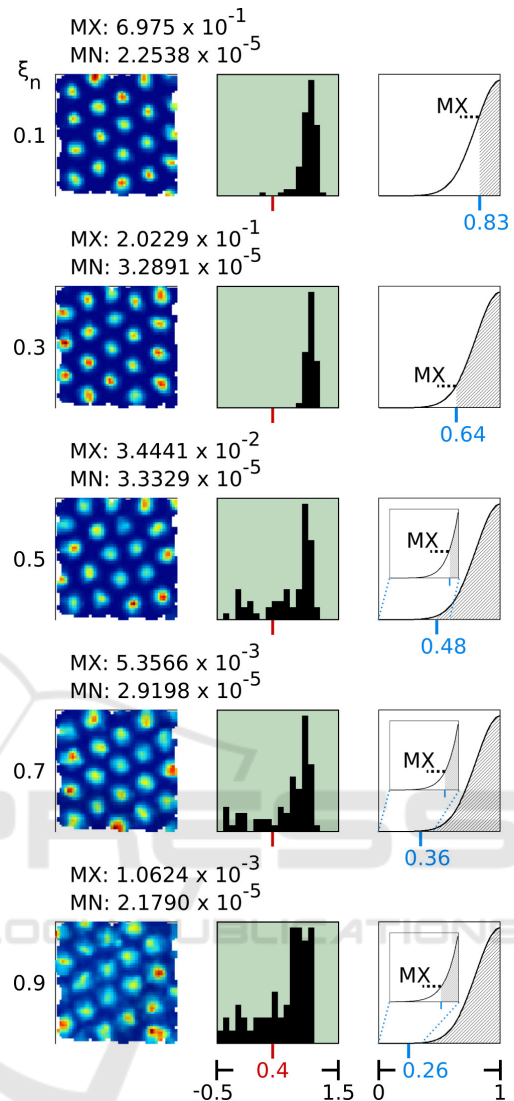


Figure 5: Artificial rate maps (left), gridness distributions (middle), and activity function plots (right) of simulation runs with varying levels ξ_n of noise (rows) added to the inputs. All simulation runs used a fixed set of parameters (Table 1) and processed location inputs derived from movement data published by Sargolini et al. (Sargolini et al., 2006). Each artificial rate map was chosen randomly from the particular set of rate maps. Average maximum activity (MX) and average minimum activity (MN) across all rate maps stated above. Gridness threshold of 0.4 indicated by red marks. Values of ratio r at average maximum activity (MX) given in blue. Insets show magnified regions of the activity function where MX values are low.

sola et al. (Stensola et al., 2012) estimate that there are up to 10 different, discrete groups of grid spacings present in the MEC. Thus, as an upper bound the number of grid cells per grid cell group can be estimated as one-tenth of the total number of grid cells in layer II of the rat MEC. This number is not exactly

known. Based on empirical data it can be estimated to lie between 14200 (Gatome et al., 2010; Krupic et al., 2012) and 25000 (Hafting et al., 2005; Sargolini et al., 2006; Boccara et al., 2010) cells resulting in an upper bound for the size $\theta_1 \cdot M$ of a grid cell group to lie between 1420 and 2500 grid cells. In contrast, a lower bound for the group size can not be estimated reliably as the actual number of observed grid cells per grid cell group is quite small (< 50) in individual animals (Stensola et al., 2012; Krupic et al., 2012). Grid cell groups may be more numerous and contain fewer cells than indicated by the upper bound. However, in the context of our RGNG-based model this uncertainty appears to be noncritical. As reported by Kerdels (Kerdels, 2016) the behavior of the simulated grid cells is not influenced by the particular size of the grid cell group in any significant way. Thus, we chose a value of $\theta_1 \cdot M = 100$ as a compromise between the possibility of a few large and many small grid cell groups. For a full, detailed derivation and characterization of the other parameters we refer to Kerdels (Kerdels, 2016).

For the simulation runs reported here we used a sequence of input locations taken from recorded movement data of rats running around in a square environment while chasing food pellets. To keep the simulation runs comparable, each run used the same trajectory. The data was published by Sargolini et al. (Sargolini et al., 2006) and is available for download⁴.

Figure 5 summarizes the results of these experiments. For each run (rows) the figure shows the firing rate map of one grid cell that was randomly chosen from the simulated grid cell group, the distribution of gridness scores⁵ of all simulated cells, and an activity function plot indicating the maximum activity exhibited by any of the simulated grid cells. The exemplary rate maps and gridness score distributions indicate that the RGNG-based model is able to tolerate increasing levels $\xi_n \in \{0.1, 0.3, 0.5, 0.7, 0.9\}$ of noise without losing its ability to form the characteristic, triangular firing patterns of grid cells. However, with increasing noise level the maximum average activity (MX) present in the rate maps drops by two orders of magnitude. This decrease is clearly visible in the activity function plots shown in the right column of figure 5. Yet, the minimal difference between the maximum average activity (MX) and the minimum average activity (MN) for any given noise level ξ_n is at least two orders of magnitude, i.e., each cell's activity may be normalized with respect to the particular noise

level without much disturbance of the grid-like firing pattern.

The reduction of the maximum average activity with increasing noise levels can be explained by the ratio r used to derive each cell's activity (Fig. 2). The ratio r describes the relative distance of the current input ξ to the best matching unit s_1 and the second best matching unit s_2 . If r is close to zero, the input has roughly the same distance to unit s_1 and to unit s_2 resulting in a low activity of the corresponding neuron. If, on the other hand, r is close to one, the input is close to the best matching unit s_1 yielding a high activity of the simulated neuron. With increasing noise the probability that an input matches the prototype of the best matching unit very closely decreases substantially. Without noise all inputs originate from a lower-dimensional manifold in input space. Adding noise to these inputs moves the inputs away from this manifold in random directions creating a local, high-dimensional region surrounding the low-dimensional manifold that is prone to effects that are commonly referred to as the *curse of dimensionality*. As a consequence, each BL prototype becomes surrounded with a kind of "dead zone" for which it is unlikely that an input will originate from it. These dead zones are indicated in the right column of figure 5 as light gray areas in the activity function plots. The values of the ratio r at the border of these zones (blue marks in Fig 5) define the probable maximum activity of the corresponding neurons.

5 CONCLUSIONS

The simulation results presented here indicate that the prototype-based representation of input space utilized by our grid cell model shows a high resilience to noise present in its input signal. This means, that even input signals with very low peak firing rates around 1Hz and a corresponding large proportion of noise through spontaneous activity can be processed by our model. According to these results, we would expect that real grid cells

- can process inputs with low peak firing rates,
- may show a similar reduction in activity when the proportion of noise in their inputs is high, and
- would not suffer a degradation of their firing field geometry in such a case.

These hypothesis may be actively tested by experiments that introduce controlled noise to the input signal, e.g., by the use of optogenetics (Hausser, 2014). Alternatively, a passive comparison of the peak firing rates present in the input signal of a grid cell and the

⁴<http://www.ntnu.edu/kavli/research/grid-cell-data>

⁵The *gridness score* ($[-2, 2]$) is a measure of how grid-like the firing pattern of a neuron is. Neurons with gridness scores greater 0.4 are commonly identified as grid cell.

resulting peak firing rate of the grid cell itself may indicate a possible correlation. To the best of our knowledge no such experiments were done yet.

However, neurons are also known to have several strategies to directly compensate for noise in their input signal by, e.g., changing electrotonic properties of their cell membranes (Koch, 2004). Such adaptations could be represented in our grid cell model by normalizing ratio r with respect to the level of noise. How such a normalization could be implemented is one subject of our future research.

In addition to these neurobiological aspects the presented results also illustrate the general ability of prototype-based learning algorithms like the GNG or RGNG to learn the structure of an input space even in the presence of very high levels of noise as shown in the last row of figure 5.

REFERENCES

- Boccaro, C. N., Sargolini, F., Thoresen, V. H., Solstad, T., Witter, M. P., Moser, E. I., and Moser, M.-B. (2010). Grid cells in pre- and parasubiculum. *Nat Neurosci*, 13(8):987–994.
- Doherty, K., Adams, R., and Davey, N. (2005). Hierarchical growing neural gas. In Ribeiro, B., Albrecht, R., Dobnikar, A., Pearson, D., and Steele, N., editors, *Adaptive and Natural Computing Algorithms*, pages 140–143. Springer Vienna.
- Domnisoru, C., Kinkhabwala, A. A., and Tank, D. W. (2013). Membrane potential dynamics of grid cells. *Nature*, 495(7440):199–204.
- Fritzsche, B. (1995). A growing neural gas network learns topologies. In *Advances in Neural Information Processing Systems 7*, pages 625–632. MIT Press.
- Fyhn, M., Molden, S., Witter, M. P., Moser, E. I., and Moser, M.-B. (2004). Spatial representation in the entorhinal cortex. *Science*, 305(5688):1258–1264.
- Gatome, C., Slomianka, L., Lipp, H., and Amrein, I. (2010). Number estimates of neuronal phenotypes in layer {II} of the medial entorhinal cortex of rat and mouse. *Neuroscience*, 170(1):156 – 165.
- Giocomo, L. M. and Hasselmo, M. E. (2008). Time constants of h current in layer ii stellate cells differ along the dorsal to ventral axis of medial entorhinal cortex. *The Journal of Neuroscience*, 28(38):9414–9425.
- Giocomo, L. M., Zilli, E. A., Fransn, E., and Hasselmo, M. E. (2007). Temporal frequency of subthreshold oscillations scales with entorhinal grid cell field spacing. *Science*, 315(5819):1719–1722.
- Hafting, T., Fyhn, M., Molden, S., Moser, M.-B., and Moser, E. I. (2005). Microstructure of a spatial map in the entorhinal cortex. *Nature*, 436(7052):801–806.
- Hausser, M. (2014). Optogenetics: the age of light. *Nat Meth*, 11(10):1012–1014.
- Jacobs, J., Weidemann, C. T., Miller, J. F., Solway, A., Burke, J. F., Wei, X.-X., Suthana, N., Sperling, M. R., Sharan, A. D., Fried, I., and Kahana, M. J. (2013). Direct recordings of grid-like neuronal activity in human spatial navigation. *Nat Neurosci*, 16(9):1188–1190.
- Kerdels, J. (2016). *A Computational Model of Grid Cells based on a Recursive Growing Neural Gas*. PhD thesis, FernUniversität in Hagen, Hagen.
- Kerdels, J. and Peters, G. (2013). A computational model of grid cells based on dendritic self-organized learning. In *Proceedings of the International Conference on Neural Computation Theory and Applications*.
- Kerdels, J. and Peters, G. (2015a). Analysis of high-dimensional data using local input space histograms. *Neurocomputing*, 169:272 – 280.
- Kerdels, J. and Peters, G. (2015b). A new view on grid cells beyond the cognitive map hypothesis. In *8th Conference on Artificial General Intelligence (AGI 2015)*.
- Killian, N. J., Jutras, M. J., and Buffalo, E. A. (2012). A map of visual space in the primate entorhinal cortex. *Nature*, 491(7426):761–764.
- Koch, C. (2004). *Biophysics of Computation: Information Processing in Single Neurons*. Computational Neuroscience Series. Oxford University Press, USA.
- Krupic, J., Burgess, N., and OKeefe, J. (2012). Neural representations of location composed of spatially periodic bands. *Science*, 337(6096):853–857.
- Lingenhhl, K. and Finch, D. (1991). Morphological characterization of rat entorhinal neurons in vivo: somadendritic structure and axonal domains. *Experimental Brain Research*, 84(1):57–74.
- Mhatre, H., Gorchetnikov, A., and Grossberg, S. (2010). Grid cell hexagonal patterns formed by fast self-organized learning within entorhinal cortex (published online 2010). *Hippocampus*, 22(2):320–334.
- Pilly, P. K. and Grossberg, S. (2012). How do spatial learning and memory occur in the brain? coordinated learning of entorhinal grid cells and hippocampal place cells. *J. Cognitive Neuroscience*, pages 1031–1054.
- Podolak, I. and Bartocha, K. (2009). A hierarchical classifier with growing neural gas clustering. In Kolehmainen, M., Toivanen, P., and Beliczynski, B., editors, *Adaptive and Natural Computing Algorithms*, volume 5495 of *Lecture Notes in Computer Science*, pages 283–292. Springer Berlin Heidelberg.
- Sargolini, F., Fyhn, M., Hafting, T., McNaughton, B. L., Witter, M. P., Moser, M.-B., and Moser, E. I. (2006). Conjunctive representation of position, direction, and velocity in entorhinal cortex. *Science*, 312(5774):758–762.
- Stensola, H., Stensola, T., Solstad, T., Froland, K., Moser, M.-B., and Moser, E. I. (2012). The entorhinal grid map is discretized. *Nature*, 492(7427):72–78.
- Yartsev, M. M., Witter, M. P., and Ulanovsky, N. (2011). Grid cells without theta oscillations in the entorhinal cortex of bats. *Nature*, 479(7371):103–107.

APPENDIX

Recursive Growing Neural Gas

The recursive growing neural gas (RGNG) has essentially the same structure as the regular growing neural gas (GNG) proposed by Fritzke (Fritzke, 1995). Like a GNG an RGNG g can be described by a tuple⁶:

$$g := (U, C, \theta) \in G,$$

with a set U of units, a set C of edges, and a set θ of parameters. Each unit u is described by a tuple:

$$u := (w, e) \in U, \quad w \in W := \mathbb{R}^n \cup G, \quad e \in \mathbb{R},$$

with the *prototype* w , and the *accumulated error* e . Note that in contrast to the regular GNG the prototype w of an RGNG unit can either be a n -dimensional vector or another RGNG. Each edge c is described by a tuple:

$$c := (V, t) \in C, \quad V \subseteq U \wedge |V| = 2, \quad t \in \mathbb{N},$$

with the units $v \in V$ connected by the edge and the *age* t of the edge. The *direct neighborhood* E_u of a unit $u \in U$ is defined as:

$$E_u := \{k \mid \exists (V, t) \in C, V = \{u, k\}, t \in \mathbb{N}\}.$$

The set θ of parameters consists of:

$$\theta := \{\varepsilon_b, \varepsilon_n, \varepsilon_r, \lambda, \tau, \alpha, \beta, M\}.$$

Compared to the regular GNG the set of parameters has grown by $\theta.\varepsilon_r$ and $\theta.M$. The former parameter is a third learning rate used in the adaptation function A (see below). The latter parameter is the maximum number of units in an RGNG. This number refers only to the number of ‘‘direct’’ units in a particular RGNG and does not include potential units present in RGNGs that are prototypes of these direct units.

Like its structure the behavior of the RGNG is basically identical to that of a regular GNG. However, since the prototypes of the units can either be vectors or RGNGs themselves, the behavior is now defined by four functions. The distance function

$$D(x, y) : W \times W \rightarrow \mathbb{R}$$

determines the distance either between two vectors, two RGNGs, or a vector and an RGNG. The interpolation function

$$I(x, y) : (\mathbb{R}^n \times \mathbb{R}^n) \cup (G \times G) \rightarrow W$$

generates a new vector or new RGNG by interpolating between two vectors or two RGNGs, respectively. The adaptation function

$$A(x, \xi, r) : W \times \mathbb{R}^n \times \mathbb{R} \rightarrow W$$

⁶The notation $g.\alpha$ is used to reference the element α within the tuple.

adapts either a vector or RGNG towards the input vector ξ by a given fraction r . Finally, the input function

$$F(g, \xi) : G \times \mathbb{R}^n \rightarrow G \times \mathbb{R}$$

feeds an input vector ξ into the RGNG g and returns the modified RGNG as well as the distance between ξ and the best matching unit (BMU, see below) of g . The input function F contains the core of the RGNG’s behavior and utilizes the other three functions, but is also used, in turn, by those functions introducing several recursive paths to the program flow.

$F(g, \xi)$: The input function F is a generalized version of the original GNG algorithm that facilitates the use of prototypes other than vectors. In particular, it allows to use RGNGs themselves as prototypes resulting in a recursive structure. An input $\xi \in \mathbb{R}^n$ to the RGNG g is processed by the input function F as follows:

- Find the two units s_1 and s_2 with the smallest distance to the input ξ according to the distance function D :

$$s_1 := \arg \min_{u \in g.U} D(u.w, \xi),$$

$$s_2 := \arg \min_{u \in g.U \setminus \{s_1\}} D(u.w, \xi).$$

- Increment the age of all edges connected to s_1 :

$$\Delta c.t = 1, \quad c \in g.C \wedge s_1 \in c.V.$$

- If no edge between s_1 and s_2 exists, create one:

$$g.C \Leftarrow g.C \cup \{(\{s_1, s_2\}, 0)\}.$$

- Reset the age of the edge between s_1 and s_2 to zero:

$$c.t \Leftarrow 0, \quad c \in g.C \wedge s_1, s_2 \in c.V.$$

- Add the squared distance between ξ and the prototype of s_1 to the accumulated error of s_1 :

$$\Delta s_1.e = D(s_1.w, \xi)^2.$$

- Adapt the prototype of s_1 and all prototypes of its direct neighbors:

$$s_1.w \Leftarrow A(s_1.w, \xi, g.\theta.\varepsilon_b),$$

$$s_n.w \Leftarrow A(s_n.w, \xi, g.\theta.\varepsilon_n), \quad \forall s_n \in E_{s_1}.$$

- Remove all edges with an age above a given threshold τ and remove all units that no longer have any edges connected to them:

$$g.C \Leftarrow g.C \setminus \{c \mid c \in g.C \wedge c.t > g.\theta.\tau\},$$

$$g.U \Leftarrow g.U \setminus \{u \mid u \in g.U \wedge E_u = \emptyset\}.$$

- If an integer-multiple of $g \cdot \theta \cdot \lambda$ inputs was presented to the RGNG g and $|g \cdot U| < g \cdot \theta \cdot M$, add a new unit u . The new unit is inserted “between” the unit j with the largest accumulated error and the unit k with the largest accumulated error among the direct neighbors of j . Thus, the prototype $u \cdot w$ of the new unit is initialized as:

$$u \cdot w := I(j \cdot w, k \cdot w), \quad j = \arg \max_{l \in g \cdot U} (l \cdot e), \\ k = \arg \max_{l \in E_j} (l \cdot e).$$

The existing edge between units j and k is removed and edges between units j and u as well as units u and k are added:

$$g \cdot C \Leftarrow g \cdot C \setminus \{c | c \in g \cdot C \wedge j, k \in c \cdot V\}, \\ g \cdot C \Leftarrow g \cdot C \cup \{(\{j, u\}, 0), (\{u, k\}, 0)\}.$$

The accumulated errors of units j and k are decreased and the accumulated error $u \cdot e$ of the new unit is set to the decreased accumulated error of unit j :

$$\Delta j \cdot e = -g \cdot \theta \cdot \alpha \cdot j \cdot e, \quad \Delta k \cdot e = -g \cdot \theta \cdot \alpha \cdot k \cdot e, \\ u \cdot e := j \cdot e.$$

- Finally, decrease the accumulated error of all units:

$$\Delta u \cdot e = -g \cdot \theta \cdot \beta \cdot u \cdot e, \quad \forall u \in g \cdot U.$$

The function F returns the tuple (g, d_{\min}) containing the now updated RGNG g and the distance $d_{\min} := D(s_1 \cdot w, \xi)$ between the prototype of unit s_1 and input ξ . Note that in contrast to the regular GNG there is no stopping criterion any more, i.e., the RGNG operates explicitly in an online fashion by continuously integrating new inputs. To prevent unbounded growth of the RGNG the maximum number of units $\theta \cdot M$ was introduced to the set of parameters.

$D(x, y)$: The distance function D determines the distance between two prototypes x and y . The calculation of the actual distance depends on whether x and y are both vectors, a combination of vector and RGNG, or both RGNGs:

$$D(x, y) := \begin{cases} D_{RR}(x, y) & \text{if } x, y \in \mathbb{R}^n, \\ D_{GR}(x, y) & \text{if } x \in G \wedge y \in \mathbb{R}^n, \\ D_{RG}(x, y) & \text{if } x \in \mathbb{R}^n \wedge y \in G, \\ D_{GG}(x, y) & \text{if } x, y \in G. \end{cases}$$

In case the arguments of D are both vectors, the Minkowski distance is used:

$$D_{RR}(x, y) := (\sum_{i=1}^n |x_i - y_i|^p)^{\frac{1}{p}}, \quad x = (x_1, \dots, x_n), \\ y = (y_1, \dots, y_n), \\ p \in \mathbb{N}.$$

Using the Minkowski distance instead of the Euclidean distance allows to adjust the distance measure with respect to certain types of inputs via the parameter p . For example, setting p to higher values results in an emphasis of large changes in individual dimensions of the input vector versus changes that are distributed over many dimensions (Kerdels and Peters, 2015a). However, in the case of modeling the behavior of grid cells the parameter is set to a fixed value of 2 which makes the Minkowski distance equivalent to the Euclidean distance. The latter is required in this context as only the Euclidean distance allows the GNG to form an induced Delaunay triangulation of its input space.

In case the arguments of D are a combination of vector and RGNG, the vector is fed into the RGNG using function F and the returned minimum distance is taken as distance value:

$$D_{GR}(x, y) := F(x, y) \cdot d_{\min}, \\ D_{RG}(x, y) := D_{GR}(y, x).$$

In case the arguments of D are both RGNGs, the distance is defined to be the pairwise minimum distance between the prototypes of the RGNGs’ units, i.e., *single linkage* distance between the sets of units is used:

$$D_{GG}(x, y) := \min_{u \in x \cdot U, k \in y \cdot U} D(u \cdot w, k \cdot w).$$

The latter case is used by the interpolation function if the recursive depth of an RGNG is at least 2. As the RGNG-based grid cell model has only a recursive depth of 1 (see next section), the case is considered for reasons of completeness rather than necessity. Alternative measures to consider could be, e.g., *average* or *complete* linkage.

$I(x, y)$: The interpolation function I returns a new prototype as a result from interpolating between the prototypes x and y . The type of interpolation depends on whether the arguments are both vectors or both RGNGs:

$$I(x, y) := \begin{cases} I_{RR}(x, y) & \text{if } x, y \in \mathbb{R}^n, \\ I_{GG}(x, y) & \text{if } x, y \in G. \end{cases}$$

In case the arguments of I are both vectors, the resulting prototype is the arithmetic mean of the arguments:

$$I_{RR}(x, y) := \frac{x + y}{2}.$$

In case the arguments of I are both RGNGs, the resulting prototype is a new RGNG a . Assuming w.l.o.g. that $|x \cdot U| \geq |y \cdot U|$ the components of the interpolated

RGNG a are defined as follows:

$$\begin{aligned}
 a & := I(x, y), \\
 a.U & := \left\{ (w, 0) \mid \begin{array}{l} w = I(u.w, k.w), \\ \forall u \in x.U, \\ k = \arg \min_{l \in y.U} D(u.w, l.w) \end{array} \right\}, \\
 a.C & := \left\{ (\{l, m\}, 0) \mid \begin{array}{l} \exists c \in x.C \\ \wedge u, k \in c.V \\ \wedge l.w = I(u.w, \cdot) \\ \wedge m.w = I(k.w, \cdot) \end{array} \right\}, \\
 a.\theta & := x.\theta.
 \end{aligned}$$

The resulting RGNG a has the same number of units as RGNG x . Each unit of a has a prototype that was interpolated between the prototype of the corresponding unit in x and the nearest prototype found in the units of y . The edges and parameters of a correspond to the edges and parameters of x .

$A(x, \xi, r)$: The adaptation function A adapts a prototype x towards a vector ξ by a given fraction r . The type of adaptation depends on whether the given prototype is a vector or an RGNG:

$$A(x, \xi, r) := \begin{cases} A_R(x, \xi, r) & \text{if } x \in \mathbb{R}^n, \\ A_G(x, \xi, r) & \text{if } x \in G. \end{cases}$$

In case prototype x is a vector, the adaptation is performed as linear interpolation:

$$A_R(x, \xi, r) := (1 - r)x + r\xi.$$

In case prototype x is an RGNG, the adaptation is performed by feeding ξ into the RGNG. Importantly, the parameters ε_b and ε_n of the RGNG are temporarily changed to take the fraction r into account:

$$\begin{aligned}
 \theta^* & := (r, r \cdot x.\theta.\varepsilon_r, x.\theta.\varepsilon_r, x.\theta.\lambda, x.\theta.\tau, \\
 & \quad x.\theta.\alpha, x.\theta.\beta, x.\theta.M), \\
 x^* & := (x.U, x.C, \theta^*), \\
 A_G(x, \xi, r) & := F(x^*, \xi).x.
 \end{aligned}$$

Note that in this case the new parameter $\theta.\varepsilon_r$ is used to derive a temporary ε_n from the fraction r .

This concludes the formal definition of the RGNG algorithm.

Parameterization

Each layer of an RGNG requires its own set of parameters. In case of our two-layered grid cell model

Table 1: Parameters of the RGNG-based model used throughout all simulation runs. Parameters θ_1 control the top layer RGNG while parameters θ_2 control all bottom layer RGNGs of the model.

θ_1	θ_2
$\varepsilon_b = 0.004$	$\varepsilon_b = 0.001$
$\varepsilon_n = 0.004$	$\varepsilon_n = 0.00001$
$\varepsilon_r = 0.01$	$\varepsilon_r = 0.01$
$\lambda = 1000$	$\lambda = 1000$
$\tau = 300$	$\tau = 300$
$\alpha = 0.5$	$\alpha = 0.5$
$\beta = 0.0005$	$\beta = 0.0005$
$M = 100$	$M = 20$

we use the sets of parameters θ_1 and θ_2 , respectively. Parameter set θ_1 controls the main top layer RGNG while parameter set θ_2 controls all bottom layer RGNGs. Table 1 summarizes the parameter values used for the simulation runs presented in this paper. For a detailed characterization of these parameters we refer to Kerdels (Kerdels, 2016).